

Trajectory Grouping with Curvature Regularization for Tubular Structure Tracking

Li Liu, Jiong Zhang, Da Chen, Huazhong Shu, and Laurent D. Cohen, *Fellow, IEEE*

Tubular structure tracking is an important and difficult problem in the fields of computer vision and medical image analysis. The minimal path models have exhibited its power in tracing tubular structures, by which a centerline can be naturally treated as a minimal path with a suitable geodesic metric. However, existing minimal path-based tubular structure tracing models still suffer from difficulty like the shortcuts and short branches combination problems, especially when dealing with the images with a complicated background. We introduce a new minima path-based model for minimally interactive tubular structure centerline extraction in conjunction with a perceptual grouping scheme. We take into account the prescribed tubular trajectories and the relevant curvature-penalized geodesic distances for minimal paths extraction in a graph-based optimization way. Experimental results on both synthetic and real images prove that the proposed model indeed obtains outperformance comparing to state-of-the-art minimal path-based tubular structure tracing algorithms.

Index Terms—Tubular structure tracking, minimal path, perceptual grouping, curvature regularization

I. INTRODUCTION

Tracking the centerlines of tubular structures such as blood vessels, roads and rivers is a fundamental task in computer vision, medical imaging and remote sensing. A basic objective for tubular structure tracking is to search for the centerline and/or the tubular boundaries in both sides to delineate an elongated structure. This is very often carried out by investigating the tubular anisotropy and appearance features to identify the centerline positions. These tubular features in general can be extracted through various multi-scale and multi-orientation filters as reviewed in [1], [2]. The existing tubular structure tracking approaches can be roughly divided into two categories: automatic tracking models for which all the branches are expected to be detected, and interactive models where the user-intervention is often taken into consideration. In this paper, we focus on the minimally interactive tracking manner.

A simple and effective idea for automatic tubular structure tracking is implemented by a path growing method. The centerline of each vessel branch is depicted by a locally optimal path propagated from a set of seed points in conjunction with a local tubular features detection procedure [3], [4], [5]. Unfortunately, the path growing approaches may fail to detect tubular structures in the presence of gaps, since the objective path can only advance a small step. The implementation of minimal paths is an alternative solution for tracking a con-

nected tubular structure tree. Significant examples include the keypoints-based minimal path growing models [6], [7], where new source points are iteratively added during the geodesic distance computation. The geodesic voting methods [8], [9] for which the tubular tree can be identified via voting score, and the minimum spanning tree model [10] where a tubular structure tree can be identified by finds saddle points from the geodesic distance map [11]. Other interesting tubular structure centerline tracing approaches include the curve evolution-based models [12], [13], the tracing algorithms relying on prescribed trajectories [14], [15], [16] and the learning-based tubularity tracking models [17], [18].

Even through they have been extensively studied, the semi- or fully automatic tubularity tracking models still lack sufficient accuracy and reliability, especially in the case of complex scenario. As an alternative solution, the type of interactive tubular centerline tracing approaches very often relies on the user intervention such as seed points which define the source and end points for tubular branch. The minimal path models, first introduced by [19], are regarded as one of the most successful tools in tracing tubular structures. However, in its original formulation [19], there is no guarantee that the minimal paths pass through the exact tubular centerlines. In order to address this issue, a two-stage procedure [20] is proposed to get the exact centerlines by taking into account the tubularity segmentation to generate centralized potential. Significant improvement on tracing the centerlines and boundaries has been made by [21], [22], where an abstract dimension representing the thickness of tubular structures is added, thus a 2D (resp. 3D) vessel can be described by a 3D (resp. 4D) minimal path. However, the short branches combination and shortcuts problems may often occur for these minimal path models, due to the complicated situation. The minimal path models [23], [24] with a dynamic metric update scheme incorporate the update procedure of geodesic metrics during the fronts propagation. The curvature regularization is introduced to minimal path computation in either continuous domain [25], [26] or discrete domain [27], leading to geodesic

Li Liu is with School of Computer Science and Technology, Donghua University, Shanghai, China.

Jiong Zhang is with USC Stevens Neuroimaging and Informatics Institute, Keck School of Medicine of USC, University of Southern California, 2025 Zonal Ave. Los Angeles, CA 90033.

Da Chen is with Qilu University of Technology (Shandong Academy of Sciences), Shandong Computer Science Center (National Supercomputer Center in Jinan), Shandong Artificial Intelligence Institute, China.

Huazhong Shu is with the Laboratory of Science and Technology, the Key Laboratory of Computer Network and Information Integration (Southeast University), Ministry of Education, 210096 Nanjing, China.

Laurent D. Cohen is with University Paris Dauphine, PSL Research University, CNRS, UMR 7534, CEREMADE, 75016 PARIS, FRANCE.

Corresponding author: Da Chen(email:chenda@ceremade.dauphine.fr

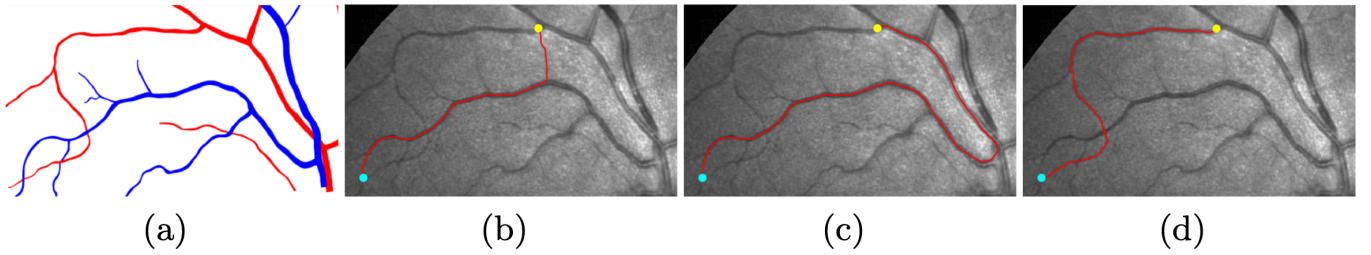


Fig. 1. Examples for shortcuts and short branches combination problems. (a) Red and blue color indicate the retinal artery and vein vessels. The objective is to extract the artery vessel between two given points indicated by dots. (b) to (d) Vessel extraction results via anisotropic minimal path model, the Finsler variant of the Sub-Riemannian minimal path model and the proposed method, respectively. The shortcuts and short branches combination problems are observed in figures b and c, while the path from the proposed passes through the correct vessel.

paths with rigid enhancement to reduce the risk of short branches combination and shortcuts problems. Unfortunately, the minimal path models mentioned above are difficult to benefit from the prescribed trajectories and may cost expensive computation burden in the sense of interactive tubular structure tracking. Despite the efforts on the improvement of minimal path techniques, the short branches combination problem still occurs when dealing with complicated situation, as depicted in Fig. 1. Figs. 1b and 1c present the results derived from the anisotropic model [22] and the progressive model [24], where one can observe short branches combination issues. While the proposed model indeed obtains good results, see Fig. 1d. It is worth to pointing out the graph-based shortest path methods [28], [29] for tubular trajectory tracing also obtain promising results.

In this paper, we propose a new minimal path model for minimally interactive tubular structure centerline tracing. It combines both the curvature-penalization geodesic distance and a set of prescribed tubular trajectories. These trajectories can be simply derived from the tubular structure segmentation by applying morphological filters. In [29], the authors present a shortest path-based tubular structure tracking model, which also relies on prescribed trajectories. However, the proposed method differs to [29] mainly at the way of establishing the connection between two trajectories which are likely. Specifically, the model in [29] connects two neighbouring trajectories using a straight segment and measures the connection cost by the length of the segment and the related angles. The corresponding cost for this connection is estimated using its Euclidean length weighted by the relevant angles. While in the proposed model, the gap between two neighbouring trajectories is recovered by a curvature-penalized geodesic path, which is more accurate and natural.

The manuscript is organized as follows. In Section II, we briefly introduce the background on the curvature-penalized minimal path model. Section III formulate the main contribution of this manuscript. The experimental results and the conclusion are presented in Sections IV and V.

II. BACKGROUND ON CURVATURE-PENALIZED MINIMAL PATH

The original isotropic minimal path model introduced by [19] is designed to search for the global minimum of a weighted curve length associated to a potential, which

is a function of low values around the image features. In tubular structure tracking applications, these features of interest are usually tubular centerline positions. The curvature-penalized minimal path approaches, such as the Finsler elastica model [25], [30] and the Finsler variant of the sub-Riemannian (FSR) models [26], are regarded as two elegant extensions to the original isotropic model. In both approaches, the curvature values of geodesic paths are taken into consideration for regularization, thus able to yield minimal paths with strongly smooth and rigid properties. The proposed tubular structure tracking model partially relies on the curvature-regularized geodesic distance and we choose the FSR metric to estimate the distance due to the low computation complexity. We refer to [31] for more analysis on the comparison between the Finsler elastica minimal path model and the FSR minimal path model.

Let $\tilde{\Omega} := \Omega \times \mathbb{S}^1$ be an orientation-lifted space, where $\Omega \subset \mathbb{R}^2$ is an open and bounded image domain and $\mathbb{S}^1 = [0, 2\pi)$ is an interval with periodic boundary condition. A core component for the FSR minimal paths computation is the data-driven geodesic metric $\mathcal{F}_{\epsilon, \beta} : \tilde{\Omega} \times \mathbb{R}^3 \rightarrow \mathbb{R}^+$, where $\epsilon \in \mathbb{R}^+$ and $\beta \in \mathbb{R}^+$ are two constant parameters. For any orientation-lifted point $\tilde{x} = (x, \theta) \in \tilde{\Omega}$ and any vector $\tilde{\mathbf{u}} = (\mathbf{u}, \nu) \in \mathbb{R}^3$, the metric $\mathcal{F}_{\epsilon, \beta}$ can be expressed as

$$\mathcal{F}_{\epsilon, \beta}(\tilde{x}, \tilde{\mathbf{u}}) = \mathcal{C}(\tilde{x}) \mathfrak{F}_{\epsilon, \beta}(\tilde{x}, \tilde{\mathbf{u}}), \quad (1)$$

where $\mathcal{C} : \tilde{\Omega} \rightarrow \mathbb{R}^+$ is an orientation-dependent function derived from the image data. In tubular structure tracking, \mathcal{C} can be derived from the orientation score estimated by a steerable filter like the optimally oriented flux (OOF) model [32]. The function $\mathfrak{F}_{\epsilon, \beta}$, which is referred to as the FSR metric, can be written as

$$\begin{aligned} \mathfrak{F}_{\epsilon, \beta}(\tilde{x}, \tilde{\mathbf{u}})^2 = & |\langle \mathbf{u}, \mathbf{n}_\theta \rangle|^2 + \beta |\nu|^2 + \epsilon^{-2} (\|\mathbf{u}\|^2 - |\langle \mathbf{u}, \mathbf{n}_\theta \rangle|^2) \\ & + (\epsilon^{-2} - 1) \min\{0, \langle \mathbf{u}, \mathbf{n}_\theta \rangle\}^2, \end{aligned} \quad (2)$$

where $\mathbf{n}_\theta = (\cos \theta, \sin \theta)$ is a vector related to θ . The parameter β dominates the importance of the curvature-based penalization.

Given the geodesic metric $\mathcal{F}_{\epsilon, \beta}$, the FSR minimal path model aims to minimize a weighted curve length $\mathcal{L}(\gamma)$ measured along a regular curve $\gamma : [0, 1] \rightarrow \Omega$ with second-order derivative

$$\mathcal{L}(\gamma) = \int_0^1 \mathcal{F}_{\epsilon, \beta}(\gamma(u), \gamma'(u)) du. \quad (3)$$

The geodesic distance map very often lends itself to the minimization of the weighted curve length \mathcal{L} . For a fixed source point $\tilde{a} \in \tilde{\Omega}$, the geodesic distance map defines a minimal curve length for each point $\tilde{x} \in \tilde{\Omega}$

$$\mathcal{U}_{\tilde{a}}(\tilde{x}) := \inf_{\gamma} \{ \mathcal{L}(\gamma), \gamma(0) = \tilde{a}, \gamma(1) = \tilde{x} \}.$$

It is known that the geodesic distance map $\mathcal{U}_{\tilde{a}}$ satisfies the Eikonal equation such that $\mathcal{U}_{\tilde{a}}(\tilde{a}) = 0$ and for any orientation-lifted point $\tilde{x} \in \tilde{\Omega} \setminus \{\tilde{a}\}$ we have

$$\mathcal{F}_{\epsilon, \beta}^*(\tilde{x}, \nabla \mathcal{U}_{\tilde{a}}(\tilde{x})) = 1, \quad (4)$$

where $\mathcal{F}_{\epsilon, \beta}^*$ is the dual metric of $\mathcal{F}_{\epsilon, \beta}$ with a form of

$$\mathcal{F}_{\epsilon, \beta}^*(\tilde{x}, \tilde{\mathbf{u}}) = \max_{\tilde{\mathbf{v}} \neq \mathbf{0}} \frac{\langle \tilde{\mathbf{u}}, \tilde{\mathbf{v}} \rangle}{\mathcal{F}_{\epsilon, \beta}(\tilde{x}, \tilde{\mathbf{v}})}.$$

The Eikonal equation (4) can be solved by using the state-of-the-art Finsler variant of the fast marching method [31]. A geodesic path $\mathcal{G}_{\tilde{a}, \tilde{x}}$ linking from \tilde{a} to \tilde{x} can be derived by reparameterizing the solution $\hat{\mathcal{G}}$ (which is also a geodesic path) to a gradient descent ordinary differential equation on $\mathcal{U}_{\tilde{a}}$

$$\hat{\mathcal{G}}(u) = \arg \max_{\|\tilde{\mathbf{v}}\|=1} \left\{ \frac{\langle \tilde{\mathbf{v}}, \nabla \mathcal{U}_{\tilde{a}}(\hat{\mathcal{G}}(u)) \rangle}{\mathcal{F}_{\epsilon, \beta}(\hat{\mathcal{G}}(u), \nabla \mathcal{U}_{\tilde{a}}(\hat{\mathcal{G}}(u)))} \right\}. \quad (5)$$

The metric $\mathfrak{F}_{\epsilon, \beta}$ implicitly encodes the curvature penalization, leading to the fact that the FSR minimal paths are the approximate minimizers to the cost $\int_0^1 \sqrt{1 + \beta \kappa(u)^2} \|\gamma'(u)\| du$ with an *irreversible* constraint on geodesic paths, where $\kappa : [0, 1] \rightarrow \mathbb{R}$ is the curvature of γ . For two given points with tangents, the minimal paths associated to the data-driven FSR metric $\mathcal{F}_{\epsilon, \beta}$ or the FSR metric $\mathfrak{F}_{\epsilon, \beta}$ tend to keep smooth, since both metrics implicitly encode curvature penalization [26] as regularization.

III. TRAJECTORY GROUPING FOR TRACING TUBULAR STRUCTURES

Motivation. In many scenarios of tubular structure tracking, the objects may cross over another one with stronger appearance features (like retinal artery vessels), or may lie in a very complicated background (like roads). As a consequence, the shortcuts or short branches combination problems often occur when directly applying minimal paths [22], [21] to trace a tubular structure in those cases. Using curvature penalization may reduce the effects from the stronger neighbouring or intersecting tubular structures. In Fig. 2 we show such an example on a synthetic image which involves two tubular structures crossing one another. As depicted in Fig. 2c, the FSR minimal path indicated by a blue line indeeds find a curve without sharp turnings under the constraint of the initial and end tangents (red arrows), satisfying the curvature penalization on these paths. In contrast, the minimal path derived from the anisotropic tubular minimal path model passes through structures with strong appearance features but with two sharp corners.

However, the FSR minimal path model still suffers from the shortcuts and/or short branches combination problems especially when the target structures have long Euclidean

curve length values. Moreover, the computation complexity for curvature-penalized minimal path models are too high for real-time applications. In order to reduce the risk of short branches combination and shortcuts problems and achieve a real-time manner, we propose a new minimal path model for minimally interactive tubular structure tracking, in conjunction with FSR geodesic distance estimation and trajectories grouping, as depicted in Fig. 3. The smoothness property of the FSR minimal paths agrees with the requirement for connecting the gaps between two adjacent vessel segments.

Overview. The proposed tubular structure tracing model is established on a graph $\mathcal{G} = (\mathcal{V}, \mathcal{E})$, where \mathcal{V} represents the node set on the graph \mathcal{G} and \mathcal{E} stands for the edge set. We further denote by $e_{ij} \in \mathcal{E}$ the edge linking two nodes ϑ_i and $\vartheta_j \in \mathcal{V}$. Each edge e_{ij} is supported to be assigned a weight value $\omega_{ij} \in \mathbb{R}_0^+$. For simplicity, we assume that $\omega_{ij} = +\infty$ implies the node ϑ_i disconnects to ϑ_j . We focus on the indirect graph, i.e. for each pair of edges e_{ij} and e_{ji} , one has $\omega_{ij} = \omega_{ji}$. In this work, the node set \mathcal{V} is constructed by means of the prescribed tubular trajectories. These trajectories can be derived from the tubular structure segmentation in conjunction with morphological filters. Note that the tubular segmentation can be regarded as a binary image for which each point is assigned a label 1 or 0. The segmentation can be carried out by various approaches. For the sake of simplicity, we apply the OOF filter [32] for the tubular feature computation and for tubular structure segmentation. In the following, we first introduce the method for computing the tubular anisotropy and appearance features via the OOF filter [32].

A. Tubular Features Extraction

In this section, the tubular structures are supported to have *locally lower intensities* than background. Let G_σ be a Gaussian kernel with variance σ and let $\{\partial_{x_i x_j} G_\sigma\}_{i,j}$ be the Hessian matrix of the kernel G_σ . The response of the OOF filter on an image $I : \Omega \rightarrow \mathbb{R}$ at a point x and a scale $r \in [R_{\min}, R_{\max}]$ is a matrix of sized 2×2 which can be expressed as

$$\Psi(x, r) = \left(I * \begin{pmatrix} \partial_{x_1 x_1} G_\sigma & \partial_{x_1 x_2} G_\sigma \\ \partial_{x_2 x_1} G_\sigma & \partial_{x_2 x_2} G_\sigma \end{pmatrix} * \chi_r \right) (x), \quad (6)$$

where χ_r is the indicator function for a disk of radius r . As analyzed in [32], the confidence map, which indicates the likelihood of a point belonging to the tubular structures, can be computed from the eigenvalues, denoted by $\lambda_1(\cdot)$ and $\lambda_2(\cdot)$ with assumption $\lambda_1(\cdot) \leq \lambda_2(\cdot)$, of $\Psi(\cdot)$. The confidence map can be formulated as follows:

$$\psi(x) = \min_{r \in [R_{\min}, R_{\max}]} \left\{ -\frac{1}{r} \lambda_1(x, r), 0 \right\}. \quad (7)$$

Furthermore, the anisotropy features at a point x located at a tubular trajectory are the two directions tangent to that trajectory. They can be estimated using the eigenvectors $\mathbf{v}_1(x, r^*)$ of the matrix $\Psi(x, r^*)$ corresponding to the eigenvalue $\lambda_1(x, r^*)$, where r^* is the scale of the tubular structure at x .

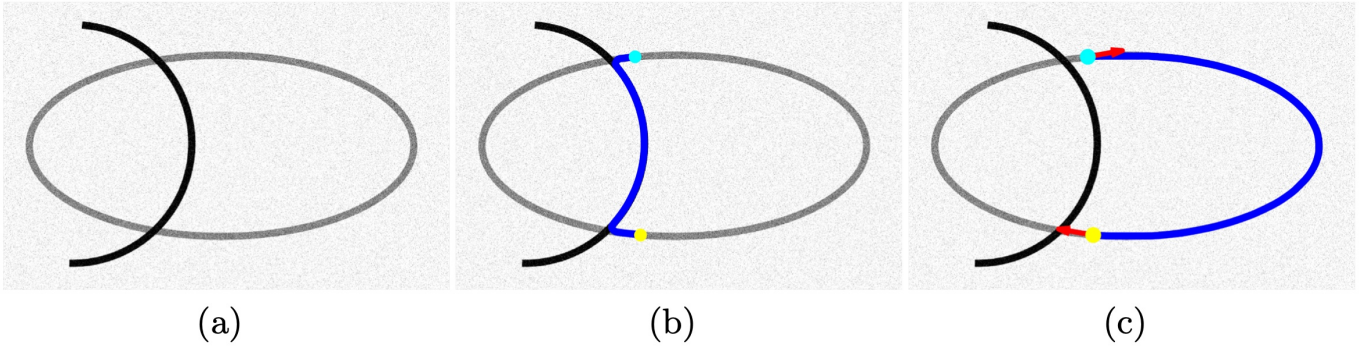


Fig. 2. (a) A synthetic image which involves two tubular structures crossing over each other. (b) and (c) Minimal paths derived from the anisotropic tubular minimal path model and the FSR model, respectively. The dots indicate the user-provided points and the blue lines represent the extracted geodesic paths

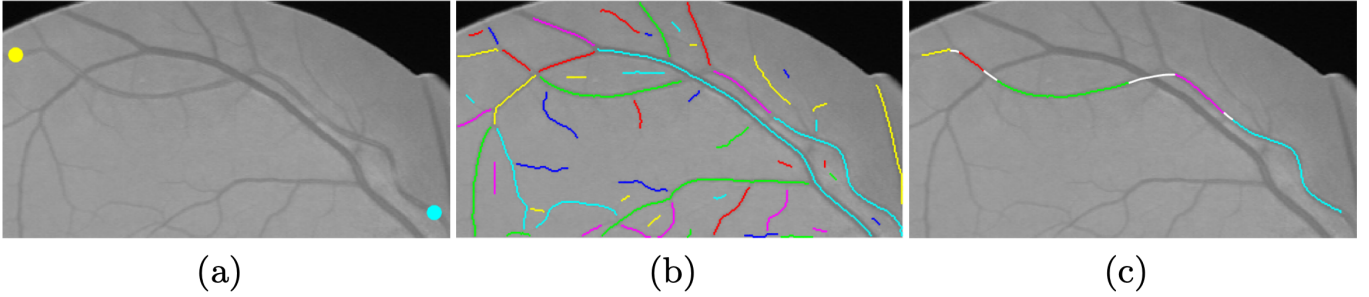


Fig. 3. The procedure of the proposed tubular structure tracing model. (a) Input image. The dots represent the user-provided points. (b) A set of trajectories superimposed on the image. (c) The grouped vessel trajectories constrained by the two dots as shown in figure (a). The white lines indicate the FSR minimal paths linking the adjacent trajectories

For each point x around the centerline positions of a tubular structure, the corresponding orientation θ_x can be estimated being such that

$$(\cos \theta_x, \sin \theta_x) \propto \mathbf{v}_1(x, r^*), \quad (8)$$

where \propto is the proportional operator.

The image data-driven function \mathfrak{C} used in Eq. 1 can be computed as

$$\mathfrak{C}(x, \theta) = \exp(\alpha \langle \mathbf{n}_\theta^\perp, \Psi(x, r^*) \mathbf{n}_\theta^\perp \rangle), \quad (9)$$

where $\alpha \in \mathbb{R}^+$ is a weighted parameter on the image data and $\mathbf{n}_\theta^\perp = (-\sin \theta, \cos \theta)$ is the orthogonal vector of \mathbf{n}_θ . Notice that the orientation-dependent scalar value $|\langle \mathbf{n}_\theta^\perp, \Psi(x, r^*) \mathbf{n}_\theta^\perp \rangle|$ can be regarded as the orientation scores.

With these definitions in hands, the tubular structure segmentation can be achieved by simply thresholding the confidence map ψ . After that we apply the morphological filters on the binary segmented tubular structures to get the skeletons of one grid point width. In order to obtain a set of separate trajectories, we remove all the branch points from the just computed tubular skeletons. An example can be seen in Fig. 3b.

B. Graph Construction

We denote by $\mathcal{T}_i \subset \Omega$ the trajectories indexed by $i \in \mathbb{N}^+$. In principle, each trajectory lies at the centerline of a tubular structure. Thus we can assign two orientations $\theta_x \in \mathbb{S}^1$ and $\theta_x + \pi \in \mathbb{S}^1$ to each point $x \in \mathcal{T}_i$, estimated via Eq. (8). Both

orientations stand for the anisotropy features that a tubular structure should have at x . In order to take these anisotropy features into consideration, we lift each trajectory \mathcal{T}_i to the orientation space $\tilde{\Omega} = \Omega \times \mathbb{S}^1$ such that the orientation-lifted trajectories are

$$\tilde{\mathcal{T}}_i = \{(x, \theta_x), (x, \theta_x + \pi); \forall x \in \mathcal{T}_i\}.$$

For the construction of a graph $\mathcal{G} = (\mathcal{V}, \mathcal{E})$, each trajectory \mathcal{T}_i can be regarded as a node so as to form the node set \mathcal{V} , see [29]. For the construction of \mathcal{E} , we should identify the neighbouring nodes for each node ϑ_i . For a trajectory \mathcal{T}_i , this can be done by building a tubular neighbourhood surrounding \mathcal{T}_i . Here we make use of the same method with [29] for identifying the neighbourhood region for each trajectory. Firstly, the trajectory \mathcal{T}_i is prolonged from its two end points along the respective tangents. Then we build a regular tubular neighbourhood M_i for extended trajectory with radius τ . A trajectory \mathcal{T}_j is said to be connected to \mathcal{T}_i with $j \neq i$, if $M_i \cap \mathcal{T}_j \neq \emptyset$.

C. Computation of the Edge Weights

Once the construction of the edge set \mathcal{E} is done, the weights $\omega_{i,j}$ for all the edges $e_{i,j}$ should be identified. In this section, a new method is introduced to estimate the weights $\omega_{i,j}$ between two connected trajectories \mathcal{T}_i and \mathcal{T}_j , i.e. two nodes ϑ_i and ϑ_j , based on the FSR metrics formulated in Eqs. (2) and (1).

The objective of this work is to group a set of trajectories $\{\mathcal{T}_i\}$ to delineate the target tubular structure. The weights $\omega_{i,j}$



Fig. 4. Qualitative comparison between different models on road image patches. The dots indicate the user-provided points and the red lines represent the obtained paths. From left to right: The results derived from the Progressive, Aniso, FSR, Eud-A and the proposed models, respectively.

should be very small when two trajectories \mathcal{T}_i and \mathcal{T}_j lie at the same tubular structure. In most scenario, the observation is that tubular structures appear to be locally smooth. In other words, a small portion of a centerline can be modeled by a curve with low curvature. Thus it is reasonable to estimate the edge weights ω_{ij} using the curvature-penalized geodesic distance.

We first define a function $\mathcal{D}_{i,j}$ measuring the minimal curvature-penalized distance from the orientation-lifted trajectories $\tilde{\mathcal{T}}_i$ to $\tilde{\mathcal{T}}_j$ via the FSR geodesic metric $\mathcal{F}_{\epsilon,\beta}$ as follows:

$$\begin{aligned} \mathcal{D}_{i,j} &= \min_{\tilde{x} \in \tilde{\mathcal{T}}_i, \tilde{y} \in \tilde{\mathcal{T}}_j} \{\mathcal{U}_{\tilde{x}}(\tilde{y})\} \\ &= \inf_{\gamma(0) \in \tilde{\mathcal{T}}_i, \gamma(1) \in \tilde{\mathcal{T}}_j} \int_0^1 \mathcal{F}_{\epsilon,\beta}(\gamma(u), \gamma'(u)) du. \end{aligned} \quad (10)$$

The distance $\mathcal{D}_{i,j}$ thus leads to a pair of points $(\tilde{x}^*, \tilde{y}^*) \in \tilde{\mathcal{T}}_i \times \tilde{\mathcal{T}}_j$ such that $\mathcal{U}_{\tilde{x}^*}(\tilde{y}^*) = \mathcal{D}_{i,j}$ and a corresponding geodesic

path $\mathcal{C}_{i,j}$ linking the point $\tilde{x}^* \in \tilde{\mathcal{T}}_i$ to $\tilde{y}^* \in \tilde{\mathcal{T}}_j$. It can be recovered by solving the gradient descent ODE (5).

Note that the distance $\mathcal{D}_{i,j}$ is weighted by the image data-driven function \mathcal{C} , which encodes the tubular appearance features. This may introduce bias to the weights $\omega_{i,j}$, especially when the target appear to be weak and simultaneously is close to stronger ones. In order to remove the bias, we propose to estimate a new curvature-dependent and image data-independent distance $\mathcal{D}_{i,j}$ as follows:

$$\begin{aligned} \mathcal{D}_{i,j} &= \int_0^1 \mathfrak{F}_{\epsilon,\beta_1}(\mathcal{C}_{i,j}(u), \mathcal{C}'_{i,j}(u)) du \\ &\approx \int_0^1 \sqrt{1 + \beta_1 \kappa_{i,j}(u)^2} du, \end{aligned} \quad (11)$$

where $\kappa_{i,j}$ is the curvature of the geodesic path $\mathcal{C}_{i,j}$ and $\beta_1 \in \mathbb{R}^+$ is a constant controlling the importance of the curvature. Note that the estimation of $\mathcal{D}_{i,j}$ by Eq. (11) allows to give

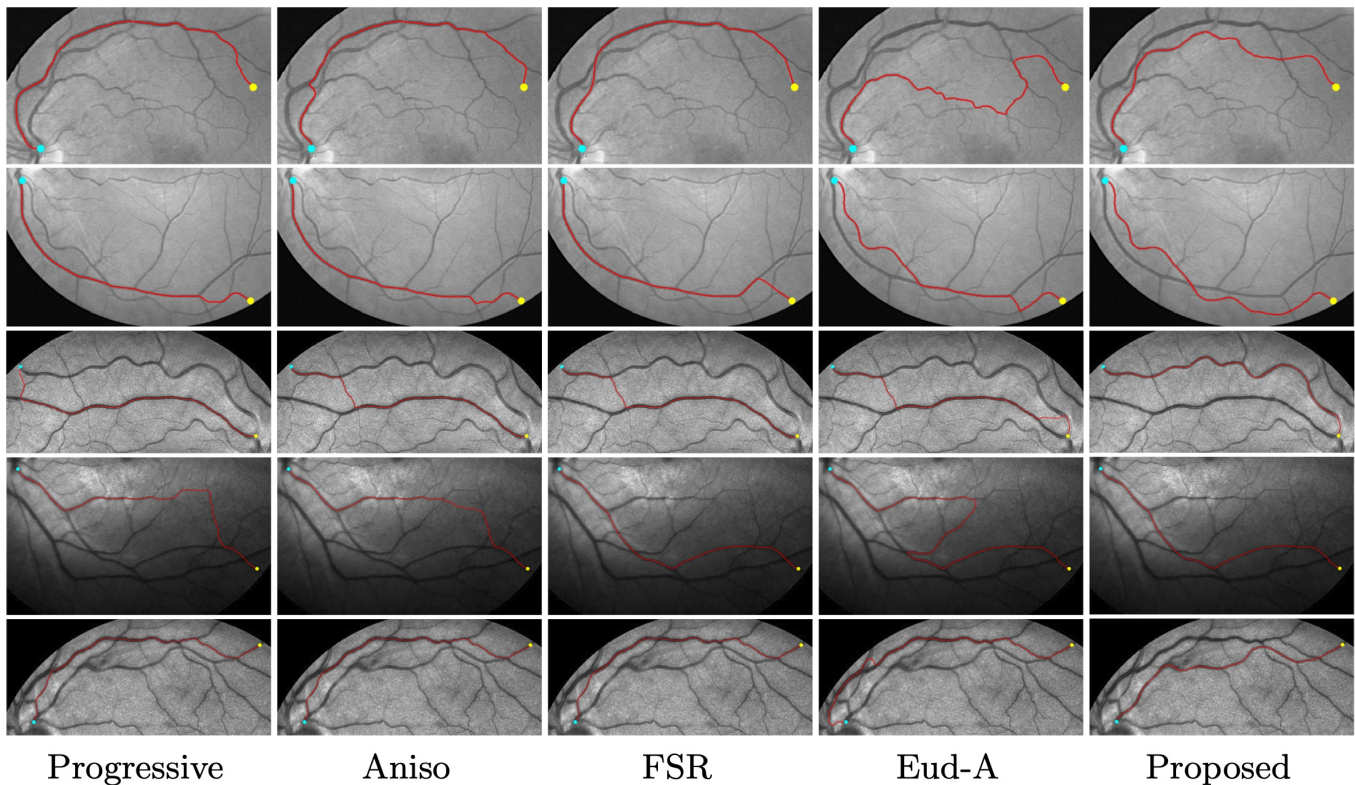


Fig. 5. Qualitative comparison between different models on Retinal image patches. The dots indicate the user-provided points and the red lines represent the obtained paths. From left to right: The results derived from the Progressive, Aniso, FSR, Eud-A and the proposed models, respectively.

more importance to the curvature penalization by setting a large value to β_1 . Similarly, we can obtain the distance from the distance $\mathcal{D}_{j,i}$ by the corresponding geodesic path $\mathcal{C}_{j,i}$ with $\mathcal{C}_{j,i}(0) \in \tilde{\mathcal{T}}_j$ and $\mathcal{C}_{j,i}(1) \in \tilde{\mathcal{T}}_i$.

Now the weight $\omega_{i,j}$ for the edge $e_{i,j}$ can be defined by

$$\omega_{i,j} = \min\{\mathcal{D}_{i,j}, \mathcal{D}_{j,i}\}. \quad (12)$$

The definition (12) imposes the symmetry property $\omega_{i,j} = \omega_{j,i}$, yielding an indirectly graph. It allows that the path linking a point \tilde{a} to \tilde{b} is equivalent to the one from \tilde{b} to \tilde{a} , thus capable of reducing user invention. Note that the path linking $\tilde{\mathcal{T}}_i$ and $\tilde{\mathcal{T}}_j$ is the one with smaller distance value.

D. Implementation

The numerical computation for $\mathcal{D}_{i,j}$ and $\mathcal{Q}_{i,j}$ can be implemented by the state-of-the-art curvature-penalized fast marching algorithm [31], which estimates the geodesic distance in a single-pass wave front propagation way. We note that the estimation for $\mathcal{D}_{i,j}$ and $\mathcal{Q}_{i,j}$ can be simultaneously carried out by expanding the front from $\tilde{\mathcal{T}}_i$ just once, since in each geodesic distance update step, the tangent of the geodesic path is also known. For each trajectory \mathcal{T}_i and a set $\{\mathcal{T}_j\}$ of neighbouring trajectories, one can compute the respective weights $\omega_{i,j}$. Once the construction of the graph is done, we can perform the Dijkstra's algorithm [33] to get the 'optimal path' which is comprised of a set of ordered and disjoint trajectories, see Fig. 3c as an example.

Since the output of the Dijkstra's algorithm is a set of separate trajectories, we need to build the final curves as

the concatenation of these order trajectories as well as the respective FSR minimal paths joining them. Here we use the similar procedure as [29] to obtain the final curve. Support that \mathcal{T}_i , \mathcal{T}_j and \mathcal{T}_k are three successive trajectories. Assume that \mathcal{T}_i and \mathcal{T}_j are linked by the FSR minimal path $\mathcal{C}_{i,j}$ subject to $\tilde{x}_i = \mathcal{C}_{i,j}(0) \in \mathcal{T}_i$ and $\tilde{x}_j = \mathcal{C}_{i,j}(1) \in \mathcal{T}_j$. Similarly, the FSR geodesic path linking \mathcal{T}_j and \mathcal{T}_k , assumed as $\mathcal{C}_{j,k}$, intersects \mathcal{T}_j at the point \tilde{y}_j . For the trajectory \mathcal{T}_j , only the portion between the two points \tilde{x}_j and \tilde{y}_j are used for the building the final curve. For each trajectory, the same procedure is applied to get the portion used for the final curve.

The computation cost for the proposed model can be divided into two parts. The first one lies at the construction of the graph, i.e. the computation of the edge weights, which indeed cost very long time. Fortunately, this process can be done offline such that the user do not have to wait online in this stage. Also, the parallel computing scheme can greatly speed up the computation. For the Dijkstra's algorithm, the computation complexity is $\mathcal{O}(N \log(N))$ where N is the total number of trajectories. Since N is much less than the number of grid points of an image, the proposed tubular structure tracking method is able to yield shortest paths in a real-time manner, after the user submits few points along the target tubular structure. The construction of the graph may cost high computation burden on the estimation for the weights $\omega_{i,j}$. However, this computation procedure can be performed offline and also can be accelerated hundreds times by parallel computing implementation.

TABLE I
AVERAGE SCORES OF \mathcal{J} FOR EVALUATING THE ARTERY VESSELS TRACING PERFORMANCE ON RETINAL COLOR IMAGES FROM THE DRIVE AND IOSTAR DATASETS

Dataset	Progressive	Aniso	FSR	Eud-A	Proposed
DRIVE	54.92%	52.26%	48.01%	84.01%	98.50%
IOSTAR	74.54%	67.09%	78.71%	85.62%	98.43%

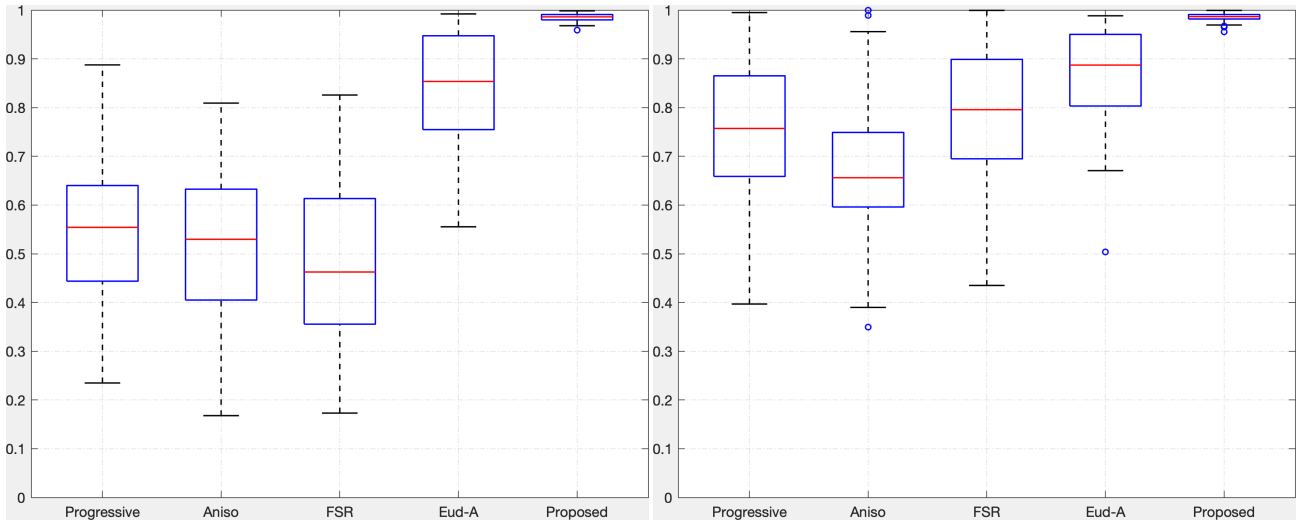


Fig. 6. Box plots of \mathcal{J} for different methods on retinal images. **Left** and **Right** Evaluation results corresponding to the DRIVE and IOSTAR datasets

IV. EXPERIMENTAL RESULTS

We conduct the numerical experiments with both qualitative and quantitative comparison to the progressive model with bending constraint (Progressive) [24], the anisotropic model (Aniso) [22], the FSR model [26], the graph-based grouping method (Eud-A) [29] on both synthetic and real images. For fair comparison, we apply the same trajectories for the Eud-A method and the proposed one.

In Figs. 4 and 5, we present the tubular structure centerline tracing results for the qualitative comparison on road and retinal images. The cyan and yellow dots respectively represent source and end points provided by user. The extracted paths are indicated by red lines. For road images, the main difficulty usually lie at the complicated background such as buildings which may also produce strong tubular appearance features. From columns 1 to 4 of Fig. 4, one can observe the shortcuts occur when implementing the compared tracing models. While for the results from the proposed model, the objective structure can be correctly traced thanks to the proposed edge weights construction way.

In Fig. 5, we show the qualitative comparison results on retinal images. The goal in this experiment is to trace the artery vessels between two points. In retinal images, the main challenge is that the artery vessels appear very weak and very often close to or even cross over strong veins. From columns 1 to 4, all the compared models suffer from both shortcuts and short branches combination problems. In contrast, the proposed model based on the curvature-penalized grouping method can obtain encouraging results.

The qualitative comparison results presented above are promising but not so sufficient. In order to make a genuine evaluation, we conduct the quantitative evaluation on DRIVE [34] and IOSTAR [35] retinal vessel datasets, by tracing artery vessels using few user-provided points. As discussed above, this is a challenging task thus can well measure the performance of the models. We consider an accuracy score defined as

$$\mathcal{J} = \frac{\#\mathbb{S} \cap \mathbb{G}}{\#\mathbb{S}},$$

where \mathbb{S} is the set of grid points passed through by the evaluated paths, \mathbb{G} denotes the region of artery vessels from the artery-vein ground truth, and $\#\mathbb{S}$ stands for the elements involved in the set \mathbb{S} . Each individual artery vessel is tracked in the whole image. In each test, all the evaluated models are under the same user-supplied points. In Table. I, we illustrate the average accuracy scores for different models on tracing artery vessels on both DRIVE and IOSTAR datasets. We made use of 394 artery vessels sampled from two datasets, where most of the major artery vessels in each retinal image are taken into account for evaluation. Among all the tests, we provide only 2 points for 321 vessels and the remaining cases require 3 points. From Table. I, we observe that the average scores of the Eud-A model and the proposed one demonstrate large gaps to the other three models, proving the advantages of using the prescribed tubular structure segmentation. Also, in each dataset the average values of the scores \mathcal{J} for the proposed model achieve around 12% higher than the Eud-A model, thanks to the use of the curvature-penalized distance to estimate the edge weights of the graph.

TABLE II
THE VALUES OF \mathcal{J} FOR EVALUATING THE TRACING RESULTS ON THE NOISED SPIRAL IMAGES

σ_n	0.05	0.10	0.15	0.20	0.25	0.3
FSR	100%	100%	100%	97.30%	92.03%	92.21%
Eud-A	100%	100%	98.42%	96.94%	97.36%	95.53%
Proposed	100%	100%	100%	100%	100%	97.91%

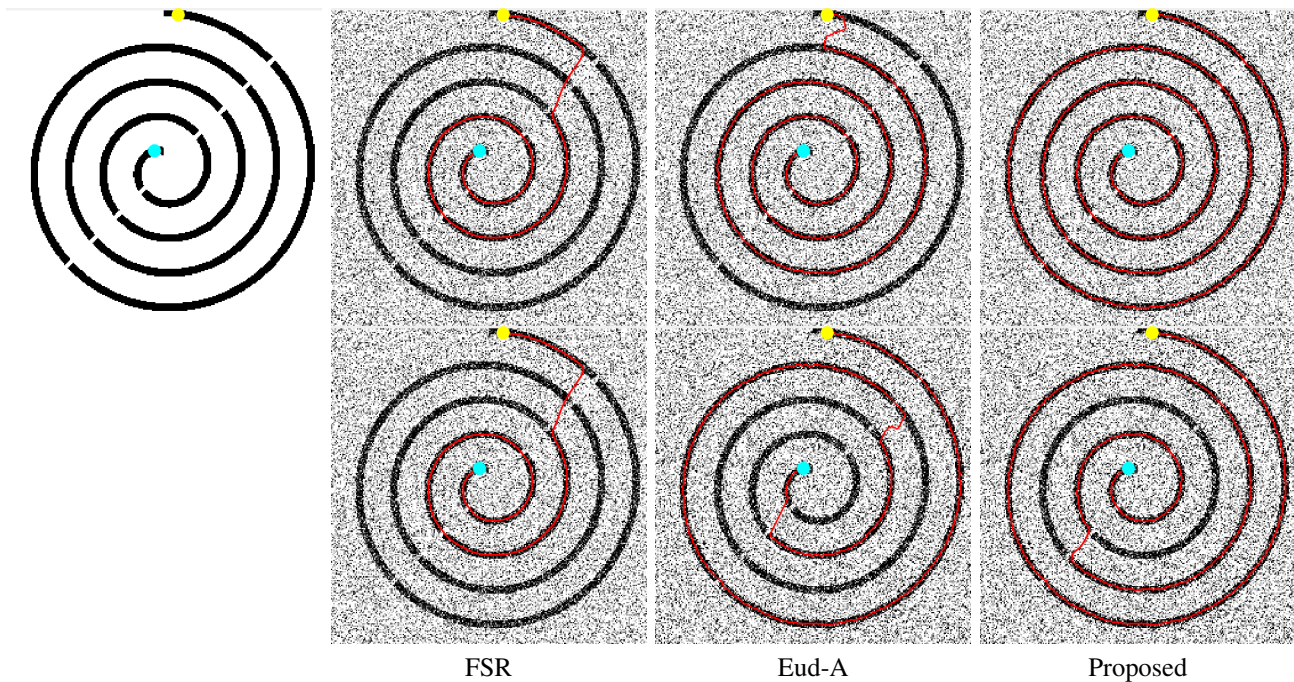


Fig. 7. The left, middle and right columns: the spiral tracking results from the Straitline model, the FSR model and the proposed one on the images with noise levels $\sigma_n = 0.25$ in the first row, and 0.3 in the second row

In Table I, only the average values of \mathcal{J} are illustrated. For better examination of the proposed model, we show more statistical results on the accuracy scores \mathcal{J} for each tested models through the tool of box plots, as depicted in Fig. 6. The left and right columns in Fig. 6 correspond to the DRIVE and IOSTAR datasets, respectively. The results shown in this figure indeed prove that the proposed model outperform the compared state-of-the-art tubular tracking models in both robustness and accuracy.

Finally, we design a synthetic spiral with several gaps which can be seen in the first column of Fig. 7. We normalize the gray levels of this synthetic image to $[0, 1]$. In this experiment, the goal is to extract the spiral between two given points denoted by dots. To examine the performance of the proposed model against the effects from noise, we add different levels of Gaussian noise, by setting the *normalized* variance as $\sigma_n = 0.05 * k$ for $k = 1, 2, \dots, 6$. The evaluation results are shown in Table. II, for which we compare to the results of the FSR and Eud-A models which are more relevant to ours. From this table, we again observe that the proposed model obtain the best performance in the sense of \mathcal{J} . Specifically, the proposed model is able to correctly extract the spiral in first five noise levels. In Fig. 7, we show the results for the FSR, Eud-A and our models on the spiral images for which the variances of the Gaussian noise are $\sigma_n = 0.25$ and 0.3. One

may observe that our model also yield shortcuts for $\sigma_n = 0.3$ due to the strong noise. This might be solved by correcting the trajectories before the graph construction.

V. CONCLUSIONS

In this paper, we propose a new minimal path model for the delineation of tubular structure trajectories in a prescribed trajectories grouping scheme based on a graph-based optimization method. The main contribution lies at the construction of the edge weights by taking in account the curve rigid property. We introduce a natural and effective way in conjunction with the curvature-penalized geodesic distance. Unlike the traditional minimal path models, the proposed one is able to blend the benefits from the prescribed tubular trajectories and the curvature-penalized geodesic paths. The experimental results prove that our model has outperformed the state-of-the-art minimal path-based tubular structure tracing models. The future work can be devoted to improve the construction of the trajectories and develop automatic algorithms based on our core idea.

ACKNOWLEDGMENT

The authors thank Dr. Jean-Marie Mirebeau from Université Paris-Sud for his fruitful discussion. This research has been

partially funded by National Natural Science Foundation of China (No. 61902224), Roche pharma (project AMD_short) and by a grant from the French Agence Nationale de la Recherche ANR-16-RHUS-0004 (RHU TRT_cSVD).

REFERENCES

- [1] S. Moccia, E. De Momi, S. El Hadji, and L. S. Mattos, "Blood vessel segmentation algorithms: Review of methods, datasets and evaluation metrics," *Comput. Methods Programs Biomed.*, vol. 158, pp. 71–91, 2018.
- [2] D. Lesage, E. D. Angelini, I. Bloch, and G. Funka-Lea, "A review of 3D vessel lumen segmentation techniques: Models, features and extraction schemes," *Med. Image Anal.*, vol. 13, no. 6, pp. 819–845, 2009.
- [3] E. Bekkers, R. Duits, T. Berendschot, and B. ter Haar Romeny, "A multi-orientation analysis approach to retinal vessel tracking," *J. Math. Imag. Vis.*, vol. 49, no. 3, pp. 583–610, 2014.
- [4] S. Cetin, A. Demir, A. Yezzi, M. Degertekin, and G. Unal, "Vessel tractography using an intensity based tensor model with branch detection," *IEEE Trans. Med. Imag.*, vol. 32, no. 2, pp. 348–363, 2013.
- [5] S. Cetin and G. Unal, "A higher-order tensor vessel tractography for segmentation of vascular structures," *IEEE Trans. Med. Imag.*, vol. 34, no. 10, pp. 2172–2185, 2015.
- [6] H. Li, A. Yezzi, and L. D. Cohen, "3D multi-branch tubular surface and centerline extraction with 4D iterative key points," in *Proc. MICCAI*, 2009, pp. 1042–1050.
- [7] E. J. Bekkers, D. Chen, and J. M. Portegies, "Nilpotent approximations of sub-Riemannian distances for fast perceptual grouping of blood vessels in 2D and 3D," *J. Math. Imag. Vis.*, vol. 60, no. 6, pp. 882–899, 2018.
- [8] Y. Rouchdy and L. D. Cohen, "Geodesic voting for the automatic extraction of tree structures. Methods and applications," *Comput. Vis. Image Understand.*, vol. 117, no. 10, pp. 1453–1467, 2013.
- [9] Y. Chen et al., "Curve-like structure extraction using minimal path propagation with backtracking," *IEEE Trans. Image Process.*, vol. 25, no. 2, pp. 988–1003, 2016.
- [10] S. Moriconi et al., "Vtrails: Inferring vessels with geodesic connectivity trees," in *Proc. IPMI*, 2017, pp. 672–684.
- [11] L. D. Cohen and T. Deschamps, "Grouping connected components using minimal path techniques. application to reconstruction of vessels in 2d and 3d images," in *Proc. CVPR*, 2001, vol. 2.
- [12] V. Mohan, G. Sundaramoorthi, and A. Tannenbaum, "Tubular surface segmentation for extracting anatomical structures from medical imagery," *IEEE Trans. Med. Imag.*, vol. 29, no. 12, pp. 1945–1958, 2010.
- [13] Y. Wang, A. Narayanaswamy, and B. Roysam, "Novel 4-D open-curve active contour and curve completion approach for automated tree structure extraction," in *Proc. CVPR*, 2011, pp. 1105–1112.
- [14] A. Vandini, B. Glocker, M. Hamady, and G.-Z. Yang, "Robust guidewire tracking under large deformations combining segment-like features (SEGlets)," *Med. Image Anal.*, vol. 38, pp. 150–164, 2017.
- [15] X. Xu, M. Niemeijer, Q. Song, M. Sonka, M. K. Garvin, J. M. Reinhardt, and M. D. Abràmoff, "Vessel boundary delineation on fundus images using graph-based approach," *IEEE Trans. Med. Imag.*, vol. 30, no. 6, pp. 1184–1191, 2011.
- [16] J. Lowell, A. Hunter, D. Steel, A. Basu, R. Ryder, and R. L. Kennedy, "Measurement of retinal vessel widths from fundus images based on 2-D modeling," *IEEE Trans. Med. Imag.*, vol. 23, no. 10, pp. 1196–1204, 2004.
- [17] E. Türetken, F. Benmansour, B. Andres, P. W. Głowacki, H. Pfister, and P. Fua, "Reconstructing curvilinear networks using path classifiers and integer programming," *IEEE Trans. Pattern Anal. Mach. Intell.*, vol. 38, no. 12, pp. 2515–2530, 2016.
- [18] J. De, L. Cheng, X. Zhang, F. Lin, H. Li, K. H. Ong, W. Yu, Y. Yu, and S. Ahmed, "A graph-theoretical approach for tracing filamentary structures in neuronal and retinal images," *IEEE Trans. Med. Imag.*, vol. 35, no. 1, pp. 257–272, 2015.
- [19] L. D. Cohen and R. Kimmel, "Global minimum for active contour models: A minimal path approach," *Int. J. Comput. Vis.*, vol. 24, no. 1, pp. 57–78, 1997.
- [20] T. Deschamps and L. D. Cohen, "Fast extraction of minimal paths in 3D images and applications to virtual endoscopy," *Med. Image Anal.*, vol. 5, no. 4, pp. 281–299, 2001.
- [21] H. Li and A. Yezzi, "Vessels as 4-D curves: Global minimal 4-D paths to extract 3-D tubular surfaces and centerlines," *IEEE Trans. Med. Imag.*, vol. 26, no. 9, pp. 1213–1223, 2007.
- [22] F. Benmansour and L. D. Cohen, "Tubular structure segmentation based on minimal path method and anisotropic enhancement," *Int. J. Comput. Vis.*, vol. 92, no. 2, pp. 192–210, 2011.
- [23] D. Chen, J. Zhang, and L. D. Cohen, "Minimal paths for tubular structure segmentation with coherence penalty and adaptive anisotropy," *IEEE Trans. Image Process.*, vol. 28, no. 3, pp. 1271–1284, 2019.
- [24] W. Liao et al., "Progressive minimal path method for segmentation of 2D and 3D line structures," *IEEE Trans. Pattern Anal. Mach. Intell.*, vol. 40, no. 3, pp. 696–709, 2018.
- [25] D. Chen, J.-M. Mirebeau, and L. D. Cohen, "Global minimum for a Finsler elastica minimal path approach," *Int. J. Comput. Vis.*, vol. 122, no. 3, pp. 458–483, 2017.
- [26] R. Duits, S. P. L. Meesters, J.-M. Mirebeau, and J. M. Portegies, "Optimal paths for variants of the 2D and 3D Reeds–Shepp car with applications in image analysis," *J. Math. Imag. Vis.*, vol. 60, no. 6, pp. 816–848, 2018.
- [27] J. Ulen, P. Strandmark, and F. Kahl, "Shortest paths with higher-order regularization," *IEEE Trans. Pattern Anal. Mach. Intell.*, vol. 37, no. 12, pp. 2588–2600, 2015.
- [28] K. Poon, G. Hamarneh, and R. Abugharbieh, "Live-vessel: Extending livewire for simultaneous extraction of optimal medial and boundary paths in vascular images," in *Proc. MICCAI*, 2007, pp. 444–451.
- [29] L. Wang et al., "Interactive retinal vessel extraction by integrating vessel tracing and graph search," in *Proc. MICCAI*, 2013, pp. 567–574.
- [30] D. Chen, J.-M. Mirebeau, and L. D. Cohen, "A new finlser minimal path model with curvature penalization for image segmentation and closed contour detection," in *Proc. CVPR*, 2016, pp. 355–363.
- [31] J.-M. Mirebeau, "Fast-marching methods for curvature penalized shortest paths," *J. Math. Imag. Vis.*, vol. 60, no. 6, pp. 784–815, 2018.
- [32] M. W. Law and A. C. Chung, "Three dimensional curvilinear structure detection using optimally oriented flux," in *Proc. ECCV*, 2008, pp. 368–382.
- [33] E. W. Dijkstra, "A note on two problems in connexion with graphs," *Numer. Math.*, vol. 1, no. 1, pp. 269–271, 1959.
- [34] J. Staal et al., "Ridge-based vessel segmentation in color images of the retina," *IEEE Trans. Med. Imag.*, vol. 23, no. 4, pp. 501–509, 2004.
- [35] J. Zhang et al., "Robust retinal vessel segmentation via locally adaptive derivative frames in orientation scores," *IEEE Trans. Med. Imag.*, vol. 35, no. 12, pp. 2631–2644, 2016.